Wireless Communication at 310 GHz using GaAs High-Electron-Mobility Transistors for Detection

Stéphane Blin, Lucie Tohme, Dominique Coquillat, Shogo Horiguchi, Yusuke Minamikata, Shintaro Hisatake, Philippe Nouvel, Thomas Cohen, Annick Pénarier, Fabrice Cano, et al.

▶ To cite this version:

Stéphane Blin, Lucie Tohme, Dominique Coquillat, Shogo Horiguchi, Yusuke Minamikata, et al.. Wireless Communication at 310 GHz using GaAs High-Electron-Mobility Transistors for Detection. Journal of Computer Networks and Communications, 2013, 15 (6), pp.559-568. 10.1109/JCN.2013.000104 . hal-01019758

HAL Id: hal-01019758
https://hal.science/hal-01019758

Submitted on 20 Feb 2019

HAL is a multi-disciplinary open access archive for the deposit and dissemination of scientific research documents, whether they are published or not. The documents may come from teaching and research institutions in France or abroad, or from public or private research centers.

L'archive ouverte pluridisciplinaire HAL, est destinée au dépôt et à la diffusion de documents scientifiques de niveau recherche, publiés ou non, émanant des établissements d'enseignement et de recherche français ou étrangers, des laboratoires publics ou privés.

Wireless Communication at 310 GHz using GaAs High-Electron-Mobility Transistors for Detection

Stéphane Blin, Lucie Tohme, Dominique Coquillat, Shogo Horiguchi, Yusuke Minamikata, Shintaro Hisatake, Philippe Nouvel, Thomas Cohen, Annick Pénarier, Fabrice Cano, Luca Varani, Wojciech Knap, and Tadao Nagatsuma

Abstract: **We report on the first error-free terahertz (THz) wireless communication at 0.310 THz for data rates up to 8.2 Gbps using a 18-GHz-bandwidth GaAs/AlGaAs field-effect transistor as a detector. This result demonstrates that low-cost commercially-available plasma-wave transistors whose cut-off frequency is far below THz frequencies can be employed in THz communication. Wireless communication over 50 cm is presented at 1.4 Gbps using a uni-travelling-carrier photodiode as a source. Transistor integration is detailed, as it is essential to avoid any deleterious signals that would prevent successful communication. We observed an improvement of the bit error rate with increasing input THz power, followed by a degradation at high input power. Such a degradation appears at lower powers if the photodiode bias is smaller. Higher-data-rate communication is demonstrated using a frequency-multiplied source thanks to higher output power. Bit-error-rate measurements at data rates up to 10 Gbps are performed for different input THz powers. As expected, bit error rates degrade as data rate increases. However, degraded communication is observed at some specific data rates. This effect is probably due to deleterious cavity effects and/or impedance mismatches. Using such a system, real-time uncompressed high-definition video signal is successfully and robustly transmitted.**

Index Terms: **Communications technology, FET, HEMT, plasma waves, receivers, THz.**

I. INTRODUCTION

Wireless communication systems at data-rates exceeding tens of Gbps require carrier signals at frequencies higher than those presently used in widespread systems based on microwave-frequency carriers (mobile phones, Wi-Fi, etc.). A terahertz-based communication link is therefore a promising breakthrough solution to achieve data-rates up to 100 Gbps as described [1]–[3]. If compared to existing wireless optical communications that are based on higher-frequency carrier signals, terahertz solutions present two significant advantages for indoor communications. First, THz beams spread more easily thanks to diffraction [4], [5], as the Rayleigh length of THz beams is smaller than that of infrared beams due to its larger wavelength. Secondly, THz beams present smaller attenuation than infrared beams in a typical indoor environment, as dry and non-metallic materials are mostly transparent to THz waves. However, THz communication systems suffer from the lack of suitable sources and detectors as mentioned in [6]. Consequently, a significant effort must be devoted to the study and development of THz solid-state sources and detectors at frequencies corresponding to atmosphere absorption minima, such as 300 GHz and 650 GHz. In this paper, we investigate the use of plasma-wave detector at 310 GHz for high-data-rate wireless communication.

Presently, the most widespread detector for THz communications is the Schottky barrier diode (SBD) [1], [7]–[9], mainly due to its high sensitivity (typically few kV/W). Plasma-wave transistors are alternative solutions for THz detection with specific attractive features for high-speed communications such as (i) lower output impedance favorable to impedance matching with high-bandwidth amplifiers, (ii) easy on-chip integration with demodulation circuit, and (iii) robustness to high input THz power. High-electron-mobility transistors (HEMT) operate as envelope detectors thanks to the non-resonant plasma rectification (self-mixing effect) as detailed in [10]–[12]. Consequently, such detectors can operate in direct detection systems. Other solutions such as heterodyne detection present attractive performances in terms of minimum detection level [13]–[15]. However, they require stringent synchronization between the local oscillators of the source and detector, or specific techniques at detection to correct for synchronization mismatch. The use of a commercial HEMT for heterodyne detection has been already investigated in [16] but our paper focuses on direct detection.

In Table 1, we present a rough overview of the room-temperature performances at 300 GHz of SBD (as reported by Virginia Diode Inc. and in [17]), Si MOSFET (reported in [18]) and GaAs HEMT (reported in [19]). In terms of sensitivity, it is important to notice that such numbers only give a rough comparison between these detectors as both measurements and metrics are different. For instance, the typical SBD sensitivity is measured using a 25-dB-gain horn antenna, thus improving the collected THz power, while no horn antenna was used to evaluate transistor sensitivities. On the other hand, transistor sensitivities were calculated using the THz power which effectively illuminates the transistor surface (as proposed in [20]), while all the THz power was used to calculate the sensitivity of the SBD. However, if one calculates the transistor sensitivity as if it was measured behind an identical horn antenna and using the

Manuscript received July 1, 2013.

This work was supported by the "WITH" JST-ANR project, by CNRS and GDR-I project "Semiconductor sources and detectors of THz frequencies" in the framework of the "GIS Teralab". We acknowledge the Region of Languedoc-Roussillon through the "HERMES Platform".

S. Blin, L. Tohme, P. Nouvel, T. Cohen, A. Pénarier, F. Cano and L. Varani are with IES, UMR 5214 CNRS, Université Montpellier 2, GIS Teralab, 34095 Montpellier, France. D. Coquillat and W. Knap are with L2C, UMR 5221 CNRS, Université Montpellier 2, GIS Teralab, 34095 Montpellier, France. email: {Stephane.Blin, knap}@univ-montp2.fr.

S. Horiguchi, Y. Minamikata, S. Hisatake and T. Nagatsuma are with Graduate School of Engineering Science, Osaka University, Toyonaka, Osaka, Japan. email: nagatuma@ee.es.osaka-u.ac.jp.

1229-2370/13/$10.00 © 2013 KICS

Table 1. Reported sensitivity, noise-equivalent power (NEP) and modulation bandwidth (BW) for SBD and transistor detectors at room temperature for a 300-GHz-frequency signal.

Detector	Sensitivity	NEP (W/$\sqrt{\text{Hz}}$)	BW
SBD	few kV/W	10^{-12}	$\approx$ 20 GHz
Si MOSFET	5 kV/W	10^{-12}	n/a
GaAs HEMT	10 V/W	$< 13\times10^{-9}$	few GHz

total THz power, we would obtain sensitivities of 3.9 kV/W and 27 V/W for the Si MOSFET and the GaAs HEMT, respectively. Therefore, Table 1 remains useful because even by correcting the sensitivities their values remain of the same order of magnitude than those reported in the table. Finally, note that the reported GaAs HEMT sensitivity and NEP are worst than those of Si MOSFET, because the latter presents an integrated bow-tie antenna. However, the GaAs HEMT was mounted on microstrip lines, thus offering possible detection of amplitude-modulated signal at modulation frequencies up to 8 GHz. Therefore, the transistor can compete with SBD as a detector for THz communications in terms of sensitivity and bandwidth.

As already mentioned, detection of amplitude-modulated THz signals was recently demonstrated at 300 GHz using plasma-wave transistors for a sine-wave modulation at frequencies up to a few GHz [19]. The first data communication was demonstrated very recently using a 200-GHz carrier frequency for data rates ranging up to hundreds of Mbps [21]. In this paper, we present for the first time a 310-GHz error-free (bit error rate lower than 10^{-11}) transmission at data rates up to 8.2 Gbps using plasma-wave transistors as detectors. Such an improvement, if compared to previously reported results [19], [21], is due to an increased effective sensitivity of the transistor associated with the use of a horn antenna, along with careful electromagnetic isolation thanks to a floating-ground isolation.

II. THZ DETECTION BASED ON PLASMA WAVES

A. Plasma-Wave Detector

The interest in using nanometer field-effect transistors (FETs) for THz applications was initiated in the early 1990s by the theoretical work of Dyakonov and Shur, who predicted that the channel of a FET could act as a resonator for plasma waves [22]. It was also shown that the nonlinear properties of the 2D plasma in the transistor channel could be used for resonant detection and mixing of THz radiation [23]. Rectification and detection of THz radiation is also possible in the non-resonant case (low electron mobility) when plasma waves decay at a distance smaller than the channel length. Fig. 1 shows the principle of THz detection of transistors.When the THz radiation is collected by the transistor through the metallic gate electrode, the THz AC voltage produced between gate and source simultaneously modulates the carrier density and drift velocity in the channel. This leads to nonlinearity and, as a result, a photoresponse appears in the form of a DC voltage between source and drain. For high-carrier-mobility devices (e.g., GaAs- and GaN- based FETs at cryogenic temperatures) the THz field can create plasma waves that propagate in the channel, and resonant plasma modes can be

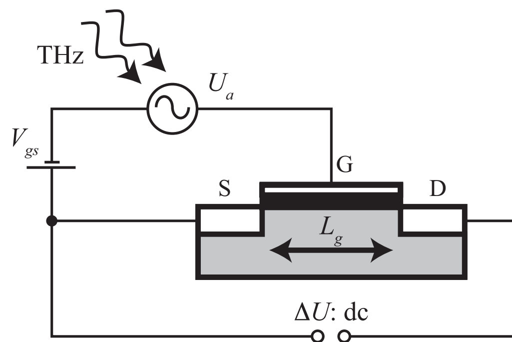

Fig. 1. Principle of THz detection based on high-electron-mobility transistor. The THz signal induces an alternating voltage U_a. The transistor sensitivity is enhanced by applying a DC voltage between gate and source. A DC voltage proportional to the input THz amplitude is measured between the source and drain pads.

excited, leading to a resonant narrowband and gate-bias-tunable detection [23]–[26]. At room temperature, plasma waves are usually overdamped and the THz radiation causes only a carrier density perturbation that decays exponentially on a distance of the order of a few tens of nanometers. A more detailed description of the physical mechanism of THz detection by FETs can be found in [27]. Currently, the most promising application appears to be room-temperature broadband THz detection in the non-resonant regime for imaging and wireless communication applications.

Different kinds of FETs, like GaAs HEMTs [24], [28], GaN HEMTs [29], InGaAs HEMTs [24], [28], [30], silicon metal-oxide-semiconductor FETs [18], [31], [32], or nanowire and graphene-based FETs [33], [34] with a gate length of the order of hundreds of nanometers exhibit good broadband THz sensitivities and can reach a NEP that is competitive with the best conventional room-temperature THz detectors. Further progress in FETs THz detection should address the improvement of the THz coupling and improvement of the transistor design. Recently, double-grating-gate field-effect transistor structures with asymmetry between source and drain to enhance the photoresponse have been designed and used for ultra-high sensitive detection and imaging at frequencies up to 2 THz [35], [36].

Moreover, FET-based THz detectors can be used to detect low-power continuous-wave THz signals due to their very good NEP, but also high-power THz pulses delivered by a free-electron laser. Therefore, their estimated damage threshold is of a few hundreds of Watts [37], that is much higher than that of SBD. Moreover, FET detectors exhibit a linear response up to an input intensity of about 1 kW/cm^2, followed by a sub-linear detection up to several MW/cm^2 [37], [38]. The saturation limit shifts to higher intensities when the frequency increases. The possibility to obtain ultrafast linear detection over a large range of powers is an important advantage for robust wireless communications.

B. Integration

Integration of transistors for successful use in communication systems is absolutely necessary for two main reasons. First, as the transistor detects the incoming THz signal coupled to the

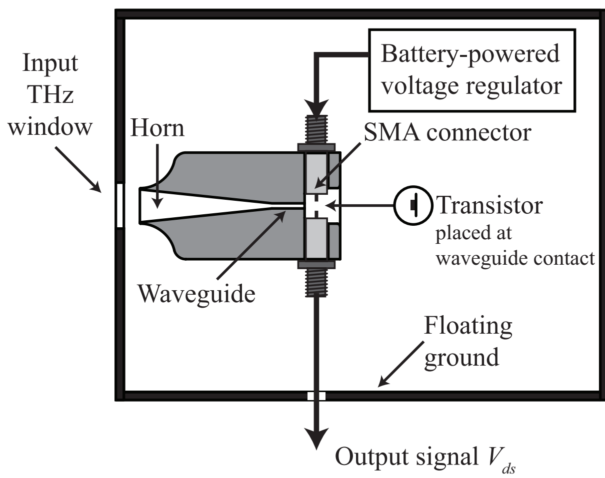

Fig. 2. Plasma-wave detector integration. A floating-ground metallic case is used for electromagnetic shielding. The transistor is placed at the waveguide output. A diagonal horn is used to collect larger THz power. The transistor is biased using a battery-powered voltage regulator placed within the shielding case.

gate, this electrode should be isolated from any other spurious electromagnetic signals to assure reasonable signal-to-noise ratio. Otherwise, HEMTs may amplify deleterious signals, especially within their typical operation bandwidths (up to few GHz or tens of GHz), which significantly degrades the signal-to-noise ratio for high-data-rate communications. Secondly, the transistor dimensions are much smaller than the diffraction-limited upcoming beam waist. Therefore, it is necessary to assure the smallest possible incoming beam waist to collect as much power as possible through the transistor surface.

In order to achieve both electromagnetic isolation and small beam waist, the HEMT is packaged as shown in Fig. 2. Improved collected THz power is assured thanks to a standard input horn. The horn was designed to have a full 3-dB beamwidth of 12° and a gain of 20 dB. The length of the horn is 26 mm with an aperture at front side of 5 mm $\times$ 5 mm. The angle of the pyramid construction is 6°. The THz signal is then concentrated on a small beam waist within a rectangular hollow waveguide (transverse dimensions equal to 432 μm $\times$ 864 μm), so that a single linear polarization is coupled to the waveguide. Integration was designed and machined thanks to digital micromachining. In order to evaluate its performances, the horn was mounted on a commercial frequency-multiplied source emitting at 290 GHz and the far-field imaging of the emitted beam was measured using a HEMT transistor as a detector. In order to improve the spatial resolution, this detector was not integrated, i.e., no input horn was used. We conducted imaging experiments in a plane orthogonal to the optical axis using 2D motorized linear stages. As shown in Fig. 3, the horn presents the expected performances, namely a symmetric Gaussian-like beam with a divergence comparable to that of Gaussian-beam simulations and a commercial horn with similar design.

Having confirmed the horn and waveguide quality, the THz detector was implemented by placing the transistor as close as possible to the waveguide output (about 500 μm). The transistor was connected to subminiature version A (SMA) connectors for biasing (gate–source voltage), and also for extracting the detected signal (drain–source voltage) produced by the incoming THz signal. In this paper, we used an ultra-low-noise GaAs pseudomorphic HEMT for detection. The transistor is packaged in a low-parasitic surface-mountable ceramic package. The top side of the cap was removed to improve detection (by suppressing the ceramic absorption) and reduce the distance between the waveguide and the transistor itself. Therefore, the top surface of the transistor (where pads are visible) was directly exposed to the incoming beam. Finally, the HEMT was shielded within a conductive enclosing to avoid electromagnetic coupling. Despite such efforts, we observed significant ground coupling issues. As a consequence, we used an external floating-ground enclosure inside which we placed both the integrated transistor and its battery-powered biasing supply.

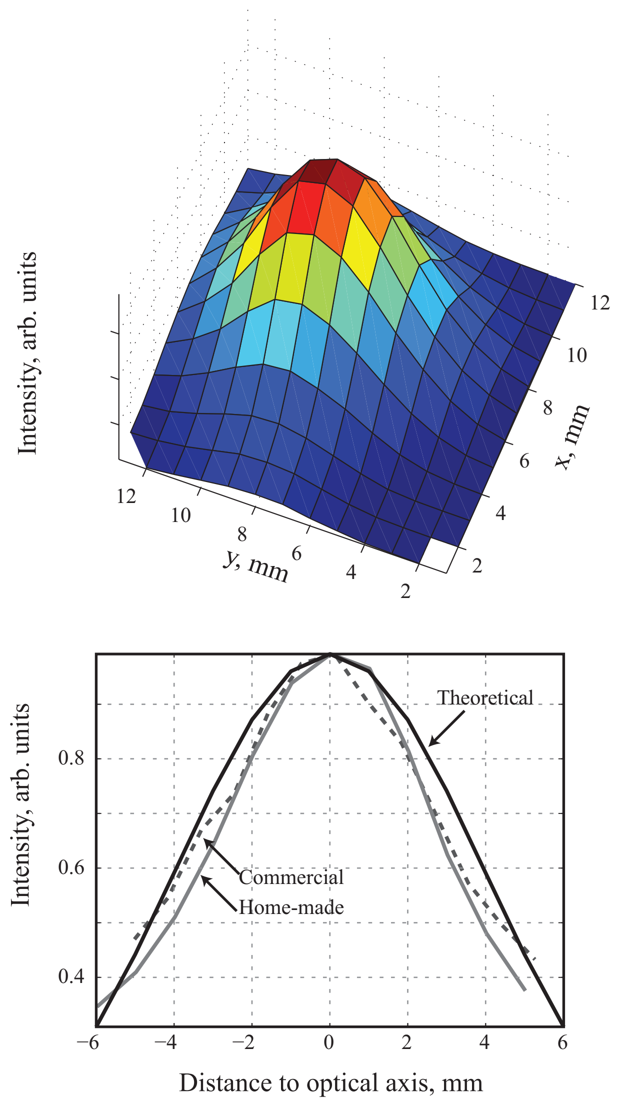

Fig. 3. Horn characterization at 290 GHz. The top graph represents the far-field intensity measured in a plane orthogonal to the optical axis for the home-made horn. The bottom graph presents a cut of the intensity along the x direction for the home-made horn and the commercial horn. The theoretical intensity is calculated using a Gaussian-beam propagation simulation.

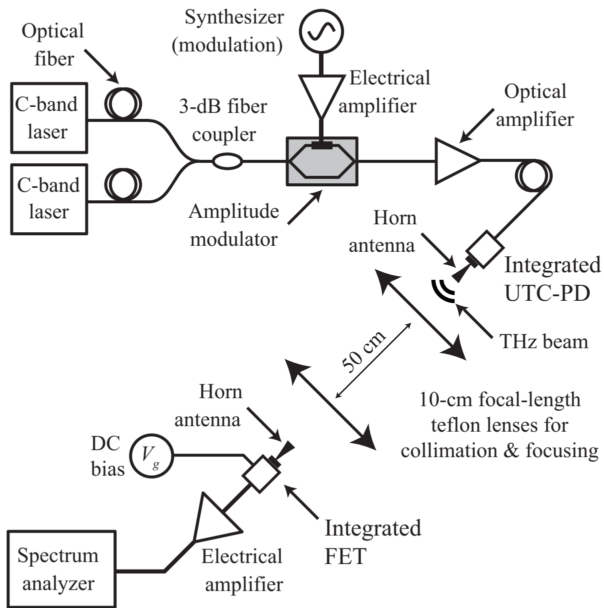

Fig. 4. Experimental setup for THz communication using the UTC-PD emitter and the plasma-wave receiver.

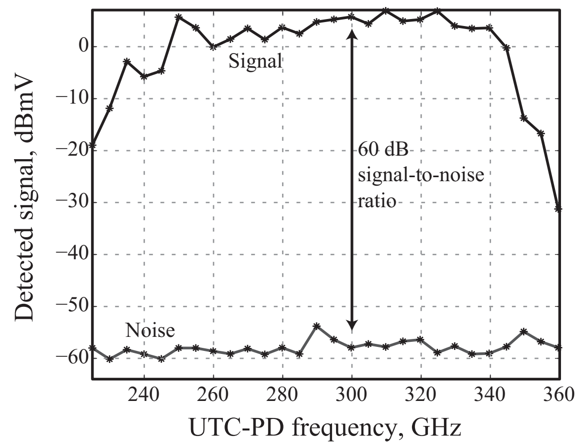

Fig. 5. Sensitivity dependence of the experimental setup. The UTC-PD emitting frequency is tuned and the detected signal at the transistor output is measured using the electrical spectrum analyzer. Noise is measured by blocking the THz signal at the transistor input window.

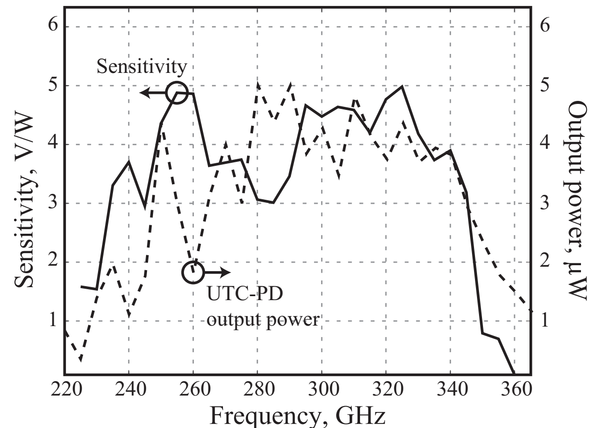

Fig. 6. HEMT sensitivity measurement. The UTC-PD output power is measured at a bias voltage of 1 V and for a photocurrent of 3 mA.

III. WIRELESS COMMUNICATION USING UTC-PD EMITTER AND HEMT DETECTOR

A. Experimental Setup

A communication link based on a uni-travelling-carrier photo-diode (UTC-PD) emitter is presented in Fig. 4. The UTC-PD emitter is excited by an optical beating generated by two continuous-wave fiber-coupled external-cavity lasers. The laser signals are coupled using a 3-dB fiber coupler then amplified using an erbium-doped fiber optical amplifier. The amplitude modulation of the optical beating is achieved using a Mach-Zehnder modulator. Precautions were taken in order to avoid any spurious radiation, especially at the modulation frequency. The critical components such as the amplitude modulator, its amplifier, and the UTC-PD are carefully packaged, thus assuring efficient shielding. The THz signal at the UTC-PD output is collimated using a 10-cm focal-length teflon lens, then focused to the HEMT using an identical lens after propagation over 50 cm. The HEMT is biased with a DC voltage between the gate and the source, and the drain-source signal produced by the incident THz beam is amplified using different kinds of amplifiers depending on the specific application such as system characterization, uncompressed high-definition (HD) video real-time transmission, or high-data-rate communications.

B. Plasma-Wave Detector Spectral Sensitivity

In order to determine the most favorable frequency of the communication link, the sensitivity of the HEMT has been measured from 220 GHz to 365 GHz. The THz signal is modulated using a sine wave at 11 MHz (minimum emitting frequency of the available synthesizer), and the detected signal is enhanced using a 40-dB-gain amplifier with an input impedance of 1 MΩ and a bandwidth of 10 MHz. The signal is observed by the electrical spectrum analyzer at 11 MHz by using a resolution bandwidth of 3 Hz. The amplitude modulation offers better accuracy than direct DC measurements. As shown in Fig. 5, the detected signal is above 0 dBmV from 250 GHz to 340 GHz, thus offering a 90-GHz bandwidth which is suitable for communications. The noise level is measured by blocking the THz beam in front of the UTC-PD emitter. Using a resolution bandwidth of 3 Hz, we measured a large signal-to-noise ratio of about 60 dB from 250 GHz to 340 GHz.

In order to evaluate the sensitivity of the transistor, the UTC-PD output power was measured using a calibrated THz power-meter based on a pyroelectric sensor. For this experiment, the sensor was directly connected to the output waveguide of the UTC-PD (after horn removal) and the optical beating was not modulated. As shown in Fig. 6, the sensitivity of the transistor is about a few volts per watt. Note that such a sensitivity is underestimated as it does not take into account the free space loss (about 4–6 dB due to absorption and reflection at teflon lenses). The sensitivity of the HEMT detector was increased thanks to the input horn, but could be further improved by 1–2 orders of magnitude using a 300-GHz antenna coupled to the gate and source terminals of the transistor, as previously re-

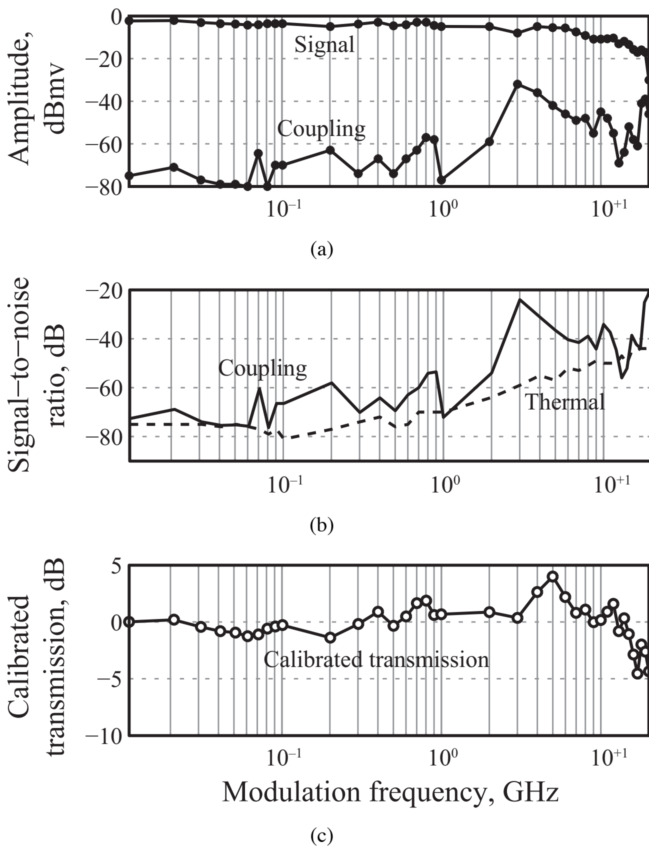

Fig. 7. Characterization of the baseband bandwidth of the plasma-wave detector: (a) presents the detected signal and remaining coupling amplitudes, the latter being measured by blocking the input THz beam, as a function of the frequency of the sine-wave amplitude modulation of the THz beam, (b) shows the signal-to-coupling and signal-to-thermal-noise ratios, the thermal noise being the white noise floor (amplifier thermal noise), and (c) shows the calibrated characterization of the plasma-wave detector after careful calibration of both modulation setup and amplifier.

ported for example on Silicon technology [18].

C. Characterization of the Baseband Modulation Bandwidth of the Plasma-Wave Detector

As shown in Fig. 5, broadband detection should allow for high-bandwidth communication. In order to evaluate such a bandwidth, the baseband modulation bandwidth of the system has been measured as shown in Fig.7. A sine modulation of the THz amplitude is applied at increasing frequencies, and the baseband signal amplitude is measured at the transistor output using an electrical spectrum analyzer. We measure the amplitude of the signal at the frequency of amplitude modulation. For these experiments, we used a 30-dB 50-Ω 18-GHz amplifier. Fig. 7(a) shows a bandwidth of about 20 GHz, in agreement with a transistor bandwidth of 18 GHz as given in the datasheet. In order to assure that such a bandwidth is not related to the amplifier at detection side, the modulation setup and the detection scheme were calibrated. The calibration measurement was conducted by sending the modulated optical signal on a high-bandwidth photodiode and amplifying the photodiode signal using the same amplifier. The calibrated characterization of the detector is represented in Fig. 7(c). We observe a detector bandwidth of about 20 GHz if measured relatively to the low-frequency plateau. The resonance observed at about 5 GHz is not clearly understood yet, but it could correspond to either an impedance mismatch and/or the presence of deleterious optical cavities.

Fig. 7(b) also shows the signal-to-noise ratio, and the signal-to-coupling ratio, where the noise is the white noise (mainly the amplifier thermal noise) and the coupling is the direct detection of the modulation signal by the transistor (without THz carrier). Even if we observe an increase of the coupling at higher modulation frequencies, the signal-to-coupling ratio exceeds 20 dB thanks to the previously-described integration, thus overpassing the direct-coupling limitation due to insufficient shielding of the experimental setup on source side and detector side [19].

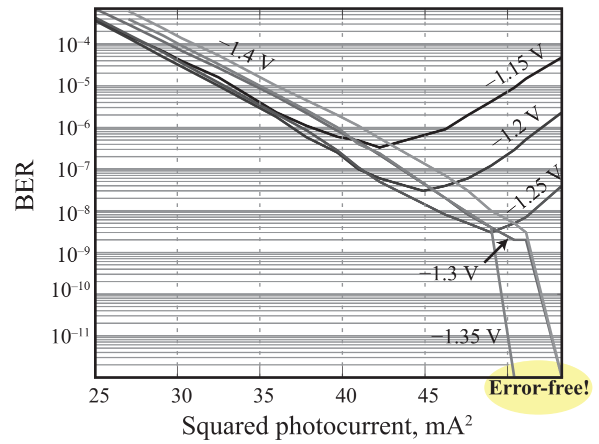

Fig. 8. BER measurement at 1.4 Gbps as a function of squared photocurrent (proportional to input THz power) at different biases of the UTC-PD. The emission frequency is 310 GHz. Error-free operation was fixed at a level of 10^{-12}.

D. Data Transmission

As the HEMT detector presents sufficient bandwidth and signal-to-noise ratio, data transmission experiments have been conducted. Even if the baseband characterization shows a good signal-to-noise ratio, this value is measured within a small bandwidth. High-data-rate communications require a large bandwidth, therefore successful communications are more challenging than detecting a sinusoidal modulation.

For communication experiments, a pseudo-random bit sequence has been used for binary on/off amplitude modulation. The bit-length sequence was limited to $2^7 - 1$ because unidentified deleterious low-frequency noise was observed at higher bit lengths. The HEMT signal was amplified using a 50-dB 50-Ω 1-GHz amplifier followed by a limiting amplifier. Error-free transmission up to 1.8 Gbps has been achieved, and the dependence on THz power and UTC-PD biasing has been evaluated as detailed in the following at a data rate of 1.38 Gbps.

THz power dependence on bit error rate (BER) was conducted by varying the input optical power at the UTC-PD emitter, and monitoring the photocurrent at the UTC-PD. As THz power is expected to be proportional to the square of the photocurrent, BER is plotted in Fig. 8 as a function of the squared photocur-

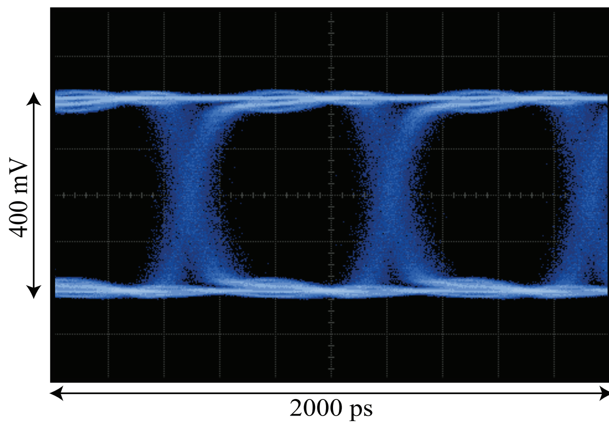

Fig. 9. Eye diagram at 1.4 Gbps using the UTC-PD source and the plasma-wave detector at 310 GHz, during an error-free (BER $< 10^{-10}$) transmission.

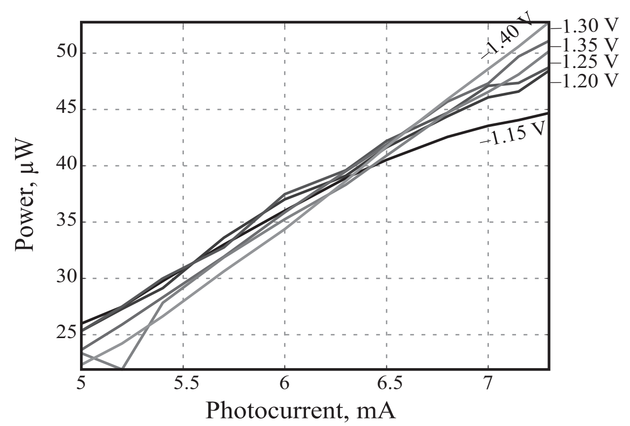

Fig. 10. Calibration of the UTC-PD emitted power for BER measurements. The output power is measured as a function of the photocurrent at different UTC-PD biases.

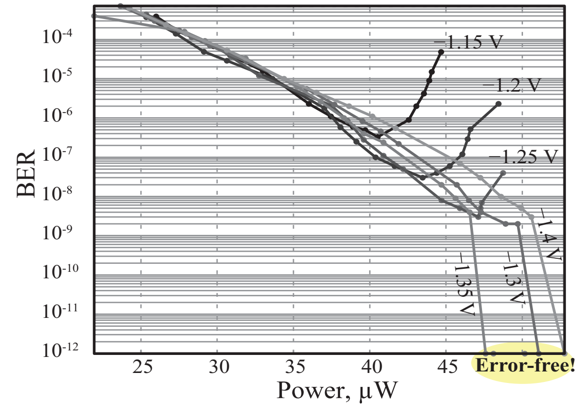

Fig. 11. BER at 310 GHz as a function of input THz power at different UTC-PD biases. The data rate is 1.4 Gbps.

rent. As can been seen in this experiment, the BER decreases as the photocurrent increases, and error-free communication is achieved at sufficiently high photocurrent, i.e. for sufficiently high THz power. Error-free operation is indicated on the figure by arbitrary choosing a value of the BER of 10^{-12} on the graph, such a value being 1–2 orders of magnitude below the minimum measurable BER. An opened eye diagram of successful error-free communication is presented in Fig. 9. At high photocurrent and low biasing of the UTC-PD, we observe in Fig. 8 a degradation of the BER. Further investigations showed that such a degradation is not correlated to a power drop but to a noise increase as will be discussed in the following.

Although an error-free communication was possible at sufficiently high source power, we observed a significant timing jitter in Fig. 9, which is much larger than that of the system (1 ps or less). This jitter contributes to the degradation of the BER. As shown in Fig. 7, the frequency response of the detector is not flat from 3 GHz to 10 GHz. Therefore, the detected eye pattern is distorted at the transistor output, and the amplitude noise is converted into jitter through the limiting amplifier. If we increase the source power and the gain of the amplifier at the transistor output, the jitter is reduced at the limiting amplifier output, as detailed in the following (see Fig. 18).

The calibration of the UTC-PD output power was carefully conducted in order to understand the origin of the BER degradation at low biasing and high photocurrents. A calibrated powermeter was used to measure the average power for various biasings at the data-rate of the experiment. Fig. 10 shows that the average output power increases with photocurrent but saturation appears at high photocurrents. Such a saturation is more evident if the bias is low, as previously shown in the case of large pulsed signals [39] or continuous-wave operation [40].

Using the previously-presented calibration, the BER can be plotted as a function of the output power as shown in Fig. 11. From this calibration, we conclude that at low power, the BER does not depend on the UTC-PD biasing. As the incident power increases, the BER reduces until a given limit where it starts degrading. This limit appears at lower powers for lower biases. Calibrated experiments allowed to identify that such a BER degradation is not related to a power drop. Further investigations were conducted by monitoring the emission spectrum of the UTC-PD using a spectrum analyzer mixer. We observed a degradation of the emission spectrum at high photocurrents, characterized by a significant increase of the white noise level. Therefore, at high photocurrents, the increase of the measured THz power with photocurrent probably corresponds to an increase of the white noise rather than to an increase of the THz carrier power.

Higher-data-rate communication should be investigated with the UTC-PD emitter and the plasma-wave receiver, but this would require a larger-bandwidth amplifier with identical gain (50 dB) in order to compensate for the limited output power of the UTC-PD and the limited sensitivity of the transistor.

IV. WIRELESS COMMUNICATION USING FREQUENCY-MULTIPLIED SOURCE AND HEMT DETECTOR

A. Communication Link

As shown in the previous section, error-free transmission at 310 GHz was demonstrated for the first time using a HEMT detector, but the data rate was limited to 1.8 Gbps due to the rela-

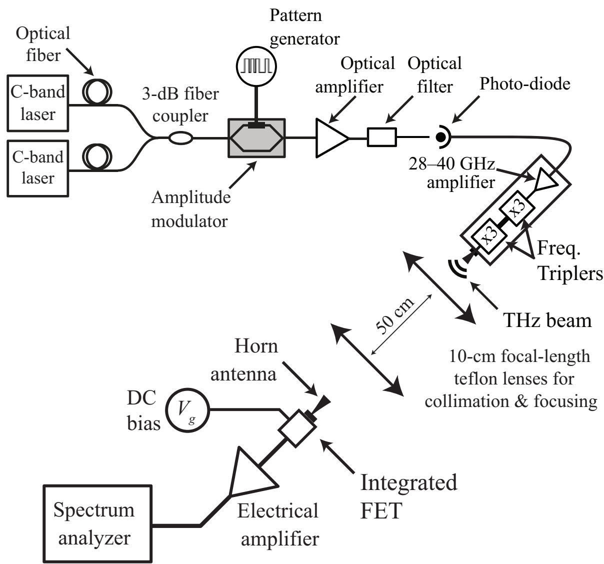

Fig. 12. Communication link using a frequency-multiplied source as emitter and a plasma-wave transistor as detector.

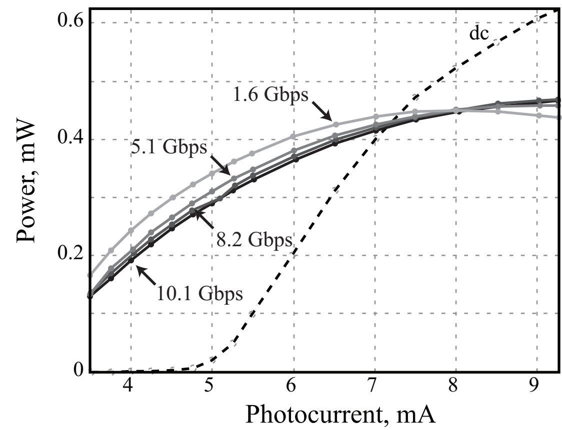

Fig. 13. Calibration of the frequency-multiplied source output THz power as a function of the driving-photodiode photocurrent at different data rates.

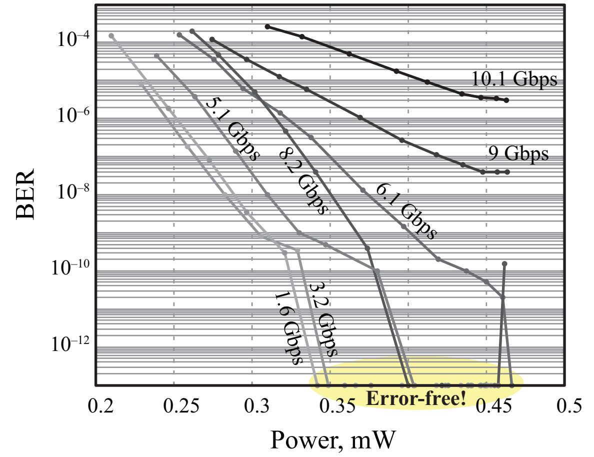

Fig. 14. Bit error rate measurements at 308.7 GHz as a function of THz power at different data rates. Error-free transmission is fixed at a level of 10^{-13}.

tively low output power of the UTC-PD emitter (about 50 μW at a photocurrent of 7.25 mA) and the limited detector sensitivity (about 4 V/W). In order to investigate communications at higher data rates, a communication link using a frequency-multiplied source has been implemented as described in Fig. 12, similarly to the one reported in [41]. The frequency-multiplication chain consists of a 28–40-GHz input amplifier, followed by two frequency triplers. This chain is driven at its input by an electrical signal which is generated by exciting a high-bandwidth photodiode with an amplitude-modulated optical beating. The optical beating generation is similar to the one previously used with the UTC-PD emitter but in this case, the optical beating frequency is of tens of GHz only as THz generation is then provided thanks to the frequency-multiplied chain. Having a frequency multiplication factor of 9, driving the chain by an optical beating within the 28–40 GHz range allows to generate a THz signal at frequencies between 250 and 360 GHz. In our experiments, we used a 34.3-GHz optical beating, thus leading to a frequency of the THz output signal of 308.7 GHz. In order to increase the signal-to-noise ratio, a 4-nm optical bandpass filter was used to reduce the amplified spontaneous emission at the amplifier output. The HEMT was biased with a DC voltage and its signal amplified using a 50-Ω 30-dB 18-GHz amplifier followed by a limiting amplifier whose output is either observed using the spectrum analyzer, a digital sampling oscilloscope or a BER measurer.

B. Calibration and BER Measurements

As discussed in the previous section, a careful calibration is delicate thus this part needs to be described in detail. As shown in Fig. 13, the output power calibration is conducted using a calibrated pyro-electric sensor both for continuous-wave emission (DC) and modulated emission. As shown in this figure, the output power is calibrated as a function of the photocurrent monitored at the photodiode. Since the calibration changes significantly as optical signal are modulated or not, we used the power calibrated using binary on/off modulated data in the following BER measurements.

Fig. 14 shows the evolution of the BER with THz power at different data rates. It exhibits the expected degradation when the THz power reduces and the data rate increases. For the first time, an error-free communication is demonstrated using a plasma-wave receiver at data rates up to 8.2 Gbps. In this experiment, error-free transmission corresponds to a BER lower than 10^{-11} and is arbitrary fixed in the figure at a level of 10^{-13}. Error-free regime is obtained for a THz power of about 350 μW at a data rate of 1 Gbps, and for 450 μW at 8.2 Gbps. One might note that a lower THz power was required when using the UTC-PD source to achieve error-free propagation (see Fig.11), as a higher-gain (20-dB more) preamplifier was used. Open eyed diagrams for error-free communication are presented in Figs. 15 and 16 at 5.3 Gbps and 8.3 Gbps, respectively.

At higher data rates (9 Gbps and 10.1 Gbps), the BER seems to reach a plateau for high THz input powers. Separate experiments were conducted in order to determine the maximum bit rate of the source and they showed a limitation at about 10 Gbps [41], mainly due to the limited bandwidth of the first

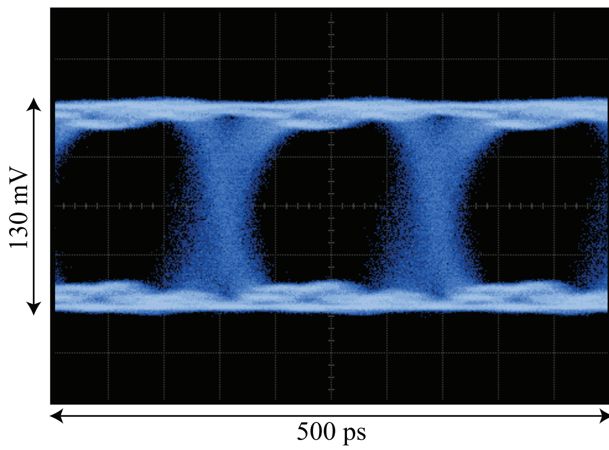

Fig. 15. Error-free (BER $< 10^{-11}$) eye diagram at 5.3 Gbps using the frequency-multiplied source and the plasma-wave receiver.

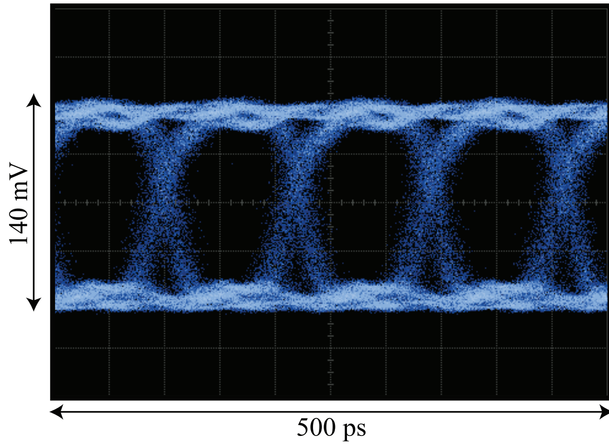

Fig. 16. Error-free (BER $< 10^{-11}$) eye diagram at 8.3 Gbps using the frequency-multiplied source and the plasma-wave receiver.

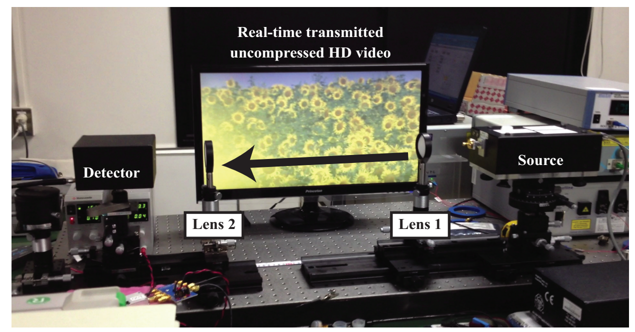

Fig. 17. Photograph of the video transmission showing the frequency-multiplied source on the right, the plasma-wave receiver on the left (inside its electromagnetic shielding box), and two teflon lenses in-between for collimation and focusing. The source amplitude is modulated by a real-time high-definition and uncompressed video signal. Transmitted signal is observed on the TV screen at the background.

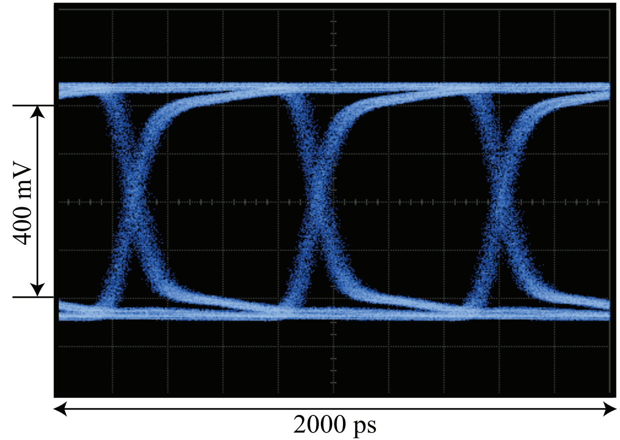

Fig. 18. Eye-diagram measured at a data rate identical to that of the high-definition uncompressed real-time video.

stage power amplifier which drives the multiplier diodes used to generate higher harmonics (3×3) in the frequency-multiplied chain. Therefore, we believe that the plateau observed at high THz input powers (see Fig. 14) and high data rate is due to a limited bandwidth of the transistor, which likely corresponds to the presence of the 5-GHz resonance that has been observed while measuring the baseband modulation bandwidth (see Fig. 7(c)).

Although error-free transmission could be obtained at high data rates, the BER was significantly degraded at some erratic data-rates. We believe that such unexpected behaviour is related to cavity effects, either between source and detector, within lenses, or within the transistor integration. Another cause could be an impedance mismatch at the transistor output. Any of these reasons or any combination of them would lead to a degradation of the BER. Further work consists in a more careful optical design in order to reduce such potentially deleterious cavity effects along with impedance matching circuit design.

C. Real-Time Uncompressed HD Video-Transmission

Since error-free communication was demonstrated at data rates of few Gbps, real-time uncompressed HD video signal should be easily transmitted as its clock frequency is around 1.5 GHz. In order to demonstrate such a transmission, the pattern generator was replaced by a DVD player whose high-definition multimedia interface (HDMI) signal was converted in a serial signal thanks to a HDMI-to-SDI converter (SDI stands for serial data interface). At the transistor output, a 50-dB 50-Ω 1-GHz pre-amplifier was used, followed by a limiting amplifier whose output was connected to a SDI-to-HDMI converter in order to observe the video on a HD TV. Successful and very robust real-time HD uncompressed video communication was observed as shown in Fig. 17. Eye-diagram at a data rate of 1.5 Gbps, i.e. at the same data rate than that of the high-definition uncompressed video signal, is shown in Fig. 18.

V. SUMMARY AND PERSPECTIVES

For the first time, high-data-rate transmission has been demonstrated using a plasma-wave transistor as a THz detector. Error-free transmission has been obtained up to 8.2 Gbps using a frequency-multiplied source and up to 1.8 Gbps using a UTC-PD source, at 310 GHz and 309 GHz, respectively, and over a distance of 50 cm. The UTC-PD-emitter output power being about an order of magnitude lower than that of the

frequency-multiplied source, achievable data rates are reduced using the former source but could be improved if the plasma-wave receiver sensitivity is increased.

Since the main drawback of using a transistor for broadband THz detection is due to its limited sensitivity and its susceptibility to deleterious electromagnetic couplings, a careful integration has been conducted in order to collect as much power as possible. The integration consists of an input diagonal horn antenna followed by a hollow waveguide, and a floating-ground shielding to reduce the detection of spurious signals.

Further work consists in improving the detector sensitivity by using a broadband antenna connected to the transistor gate and source contacts. Having an increased sensitivity is important as similar communication performances would be possible with no teflon lens or horn antenna, thus offering an integrated solution which could be used in mobile devices, computers, etc. In order to offer more robust communications using plasma-wave transistors, further work also requires (i) a careful optical design including anti-reflection coating to reduce deleterious cavity effects, (ii) an impedance-matching design between the transistor output and the amplifier, and (iii) an improvement in the electromagnetic isolation of the transistor. Additionally, more advanced modulation schemes, such as multi-level amplitude modulation, should allow to significantly increase the possible communication data rate using HEMT as THz detectors. We believe that such improvements should make plasma-wave transistors the most competitive detectors for high data-rate communications.

ACKNOWLEDGMENTS

We acknowledge Guillaume Ducournau and Jean-François Lampin from IEMN (Univ. Lille 1, France), along with Jean-François Roux (IMEP-LAHC, Univ. of Savoie, France) for preliminary experiments within the ANR-JST WITH project which helped converging towards higher electromagnetic compatibility detector.

REFERENCES

[1] H. Song and T. Nagatsuma, "Present and future of terahertz communications," *IEEE Trans. Terahertz Sci. Technol.*, vol. 1, no. 1, pp. 256–263, 2011.

[2] J. Federici and L. Moeller, "Review of terahertz and subterahertz wireless communications," *J. Appl. Physics*, vol. 107, no. 11, p. 111101, 2010.

[3] T. Kleine-Ostmann and T. Nagatsuma, "A review on terahertz communications research," *J. Infrared Milimeter Terahertz Waves*, vol. 32, no. 2, pp. 143–171, 2011.

[4] C. Jansen, S. Priebe, C. Moller, M. Jacob, H. Dierke, M. Koch, and T. Kurner, "Diffuse scattering from rough surfaces in THz communication channels," *IEEE Trans. Terahertz Sci. Technol.*, vol. 1, no. 2, pp. 462–472, 2011.

[5] T. Kürner, "Towards future THz communications systems," *Int. J. Terahertz Sci. Technol.*, vol. 1, no. 2, pp. 462–472, 2011.

[6] D. Dragoman and M. Dragoman, "Terahertz fields and applications," *Progress in Quantum Electronics*, vol. 28, no. 1, pp. 1–6, 2004.

[7] C. Jastrow *et al.*, "300 GHz transmission system," *Electron. Lett.*, vol. 44, no. 3, pp. 213–214, 2008.

[8] L. Moeller *et al.*, "2.5 Gb/s error-free transmission at 625 GHz using a narrow-bandwidth 1 mWTHz source," in *Proc. Tech. Dig. URSI General Assembly and Scientific Symposium*, 2001.

[9] K. Ishigaki *et al*, "Direct intensity modulation and wireless data transmission characteristics of terahertz-oscillating resonant tunnelling diodes," *Electron. Lett.*, vol. 48, no. 10, pp. 582–583, 2012.

[10] M. Dyakonov and M. Shur, "Detection, mixing, and frequency multiplication of terahertz radiation by two-dimensional electronic fluid," *IEEE Trans. Electron Devices*, vol. 43, no. 3, pp. 380–387, 1996.

[11] W. Knap and M. I. Dyakonov, "Field-effect transistor for terahertz applications," *Handbook of terahertz technology for imaging, sensing and communications, Woodhead Publishing Series in Electronic and Optical Materials*, no. 34, 2013.

[12] W. Knap *et al.*, "Using mobile agents for distributed network performance management," *J. Infrared Millimeter Terahertz Waves*, vol. 30, pp. 1319–1337, 2009.

[13] J. Antes, S. Konig, A. Leuther, H. Massler, J. Leuthold, O. Ambacher, and I. Kallfass, "220 GHz wireless data transmission experiments up to 30 Gbit/s," in *Proc. IEEE MTT-S International Microwave Symposium Digest (MTT)*, pp. 1–3, 2012.

[14] G. Ducournau, A. Beck, F. Pavanello, P. Latzel, T. Akalin, E. Peytavit, M. Zaknoune, and J. Lampin, "22 Gbit/s wireless link at 400 GHz using photonic transmitter and heterodyne electronic detection," in *Proc. 7th Terahertz Days*, 2013.

[15] T. J. Chung and W.-H. Lee, "10-Gbit/s wireless communication system at 300 GHz," *ETRI J.*, vol. 35, no. 3, 2013.

[16] L. Tohme, S. Blin, P. Nouvel, L. Varani, and A. Pénarier, "Room-temperature terahertz heterodyne mixing in GaAs commercial transistors," in *Proc. IRMMW-THz (Mainz, Germany)*, 2013.

[17] H.-J. Song, K. Ajito, A. Wakatsuki, Y. Muramoto, N. Kukutsu, Y. Kado, and T. Nagatsuma, "Terahertz wireless communication link at 300 GHz," in *Proc. Int. Topical Meeting Microw. Photon. (MWP)*, 2010, pp. 42–45.

[18] F. Schuster, D. Coquillat, H. Videlier, M. Sakowicz, F. Teppe, L. Dussopt, B. Giffard, T. Skotnicki, and W. Knap, "Broadband terahertz imaging with highly sensitive silicon CMOS detectors," *Optics Express*, vol. 19, no. 8, pp. 7827–7832, 2011.

[19] S. Blin, F. Teppe, L. Tohme, S. Hisatake, K. Arakawa, P. Nouvel, D. Coquillat, A. Pénarier, J. Torres, L. Varani, W. Knap, and T. Nagatsuma, "Plasma-wave detectors for terahertz wireless communication," *IEEE Electron Device Lett.*, vol. 33, no. 10, pp. 1354–1356, 2012.

[20] A. Lisauskas *et al.*, "Terahertz imaging with Si MOSFET focal-plane arrays," in *Proc. SPIE*, 2009, vol. 7215, no. 6.

[21] L. Tohme, G. Ducournau, S. Blin, D. Coquillat, P. Nouvel, A. Pénarier, W. Knap, and J. F. Lampin, "0.2 THz wireless communication using plasma-wave transistor detector," in *Proc. IRMMW-THz*, 2013.

[22] M. Dyakonov and M. Shur, "Shallow water analogy for a ballistic field effect transistor: New mechanism of plasma wave generation by dc current," *Phys. Rev. Lett.*, vol. 71, pp. 2465–2468, Oct. 1993.

[23] M. I. Dyakonov and M. S. Shur, "Plasma wave electronics: Novel terahertz devices using two dimensional electron fluid," *IEEE Trans. Electron Devices*, vol. 43, no. 10, pp. 1640–1645, 1996.

[24] J.-Q. Lu and M. S. Shur, "Terahertz detection by high-electron-mobility transistor: Enhancement by drain bias," *Appl. Physics Lett.*, vol. 78, no. 17, pp. 2587–2588, 2001.

[25] W. Knap, Y. Deng, S. Rumyantsev, and M. Shur, "Resonant detection of subterahertz and terahertz radiation by plasma waves in submicron field-effect transistors," *Appl. Physics Lett.*, vol. 81, no. 24, pp. 4637–4639, 2002.

[26] A. El Fatimy, F. Teppe, N. Dyakonova, W. Knap, D. Seliuta, G. Valusis, A. Shchepetov, Y. Roelens, S. Bollaert, A. Cappy, *et al.*, "Resonant and voltage-tunable terahertz detection in InGaAs InP nanometer transistors," *Appl. Physics Lett.*, vol. 89, no. 13, p.131926, 2006.

[27] M. Dyakonov, "Generation and detection of Terahertz radiation by field effect transistors," *Comptes Rendus Physique*, vol. 11, no. 7, pp. 413–420, 2010.

[28] S. Boubanga-Tombet, F. Teppe, D. Coquillat, S. Nadar, N. Dyakonova, H. Videlier, W. Knap, A. Shchepetov, C. Gardés, Y. Roelens, *et al.*, "Current driven resonant plasma wave detection of terahertz radiation: Toward the Dyakonov-Shur instability," *Appl. Physics Lett.*, vol. 92, no. 21, p. 212101, 2008.

[29] A. Muravjov, D. Veksler, X. Hu, R. Gaska, N. Pala, H. Saxena, R. Peale, and M. Shur, "Resonant terahertz absorption by plasmons in gratinggate GaN HEMT structures," in *Proc. SPIE DSS*, 2009, p. 73110D.

[30] P. Nouvel, H. Marinchio, J. Torres, C. Palermo, D. Gasquet, L. Chusseau, L. Varani, P. Shiktorov, E. Starikov, and V. Gruzinskis, "Terahertz spectroscopy of plasma waves in high electron mobility transistors," *J. Appl. Physics*, vol. 106, no. 1, p. 013717, 2009.

[31] R. Tauk, F. Teppe, S. Boubanga, D. Coquillat, W. Knap, Y. Meziani, C. Gallon, F. Boeuf, T. Skotnicki, C. Fenouillet-Beranger, *et al.*, "Plasma wave detection of terahertz radiation by silicon field effects transistors: Responsivity and noise equivalent power," *Appl. Physics Lett.*, vol. 89, no. 25, p. 253511, 2006.

[32] E. Ojefors, U. R. Pfeiffer, A. Lisauskas, and H. G. Roskos, "A 0.65 THz focal-plane array in a quarter-micron CMOS process technology," *IEEE J. Solid-State Circuits*, vol. 44, no. 7, pp. 1968–1976, 2009.

[33] L. Romeo, D. Coquillat, M. Pea, D. Ercolani, F. Beltram, L. Sorba, W. Knap, A. Tredicucci, and M. Vitiello, "Nanowire-based field effect transistors for terahertz detection and imaging systems," *Nanotechnol.*, vol. 24, no. 21, p. 214005, 2013.
[34] L. Vicarelli, M. Vitiello, D. Coquillat, A. Lombardo, A. Ferrari, W. Knap, M. Polini, V. Pellegrini, and A. Tredicucci, "Graphene field-effect transistors as room-temperature terahertz detectors," *Nature Materials*, 2012.
[35] T. Watanabe, S. B. Tombet, Y. Tanimoto, Y. Wang, H. Minamide, H. Ito, D. Fateev, V. Popov, D. Coquillat, W. Knap, *et al*, "Ultrahigh sensitive plasmonic terahertz detector based on an asymmetric dual-grating gate HEMT structure," *Solid-State Electron.*, 2012.
[36] V. Popov, D. Fateev, T. Otsuji, Y. Meziani, D. Coquillat, and W. Knap, "Plasmonic terahertz detection by a double-grating-gate field-effect transistor structure with an asymmetric unit cell," *Appl. Physics Lett.*, vol. 99, no. 24, p. 243504, 2011.
[37] D. But, C. Drexler, N. Dyakonova, O. Drachenko, S. Ganichev, and W. Knap, "Nonlinear photoresponse of FET THz broadband detectors at high power irradiation," in *Proc. IRMMW-THz (Mainz, Germany)*, 2013.
[38] W. Knap, S. Rumyantsev, M. S. Vitiello, D. Coquillat, S. Blin, N. Dyakonova, M. Shur, F. Teppe, A. Tredicucci, and T. Nagatsuma, "Nanometer size field effect transistors for terahertz detectors," *Nanotechnology*, vol. 24, no. 21, p. 214002, 2013.
[39] T. Ishibashi, T. Furuta, H. Fushimi, S. Kodama, T. Nagatsuma, N. Shimizu, and Y. Miyamoto, "InP/InGaAs uni-traveling-carrier photodiodes," *IEICE Trans. Electron.*, vol. 83, no. 6, pp. 938–949, 2000.
[40] A. Hirata, H. Ishii, and T. Nagatsuma, "Design and characterization of a 120-GHz millimeter-wave antenna for integrated photonic transmitters," *IEEE Trans. Microw. Theory Tech.*, vol. 49, no. 11, pp. 2157–2162, 2001.
[41] T. Nagatsuma, S. Horiguchi, Y. Minamikata, Y. Yoshimizu, S. Hisatake, S. Kuwano, N. Yoshimoto, J. Terada, and H. Takahashi, "Terahertz wireless communications based on photonics technologies," *Opt. Express*, vol. 21, pp. 23736–23747, Oct. 2013.

Stéphane Blin was born in St Nazaire, France on January 6, 1977. He received the Ph.D. degree in Physics from Enssat, Lannion, France and the Ph.D. degree in Electrical Engineering from Université Laval, Québec, Canada in 2003. From 2000 to 2004, he led original optical injection experiments at very low injection levels which led to original metrological methods, and studied frequency noise of highly-coherent lasers with DiCOS Technol. From 2004 to 2007, he was engaged in research on acoustic fiber-sensor arrays and air-core photonic-bandgap fiber-optic gyroscope at Ginzton Laboratory, Stanford University, CA. From 2007 to 2009, he worked at Foton laboratory (Enssat) on high-peak-power fiber lasers for material processing applications. Since 2009, he joined the Institut d'électronique du sud, University of Montpellier 2, France as an associate professor. His current research interests are THz-waves generation, detection, waveguides and systems.

Tadao Nagatsuma received the B.S., M.S., and Ph.D. degrees in electronic engineering from Kyushu University, Fukuoka, Japan, in 1981, 1983, and 1986, respectively. During his Ph.D. studies, he was involved in millimeter-wave and submillimeter-wave oscillators based on flux-flow phenomenon in superconducting devices. In 1986, he joined the Electrical Communications Laboratories, Nippon Telegraph and Telephone Corporation (NTT), Atsugi, Kanagawa, Japan, where he was engaged in research on the design and testing of ultrahigh-speed semiconductor electronic/photonic devices and integrated circuits. From 1999 to 2002, he was a Distinguished Technical Member with NTT Telecommunications Energy Laboratories. From 2003 to 2007, he was a Group Leader with NTT Microsystem Integration Laboratories. He is currently a Professor at the Division of Advanced Electronics and Optical Science, Department of Systems Innovation, Graduate School of Engineering Science, Osaka University, Toyonaka, Japan. His research interests include millimeter-wave, terahertz photonics, their application to sensors, and wireless communications. Prof. Nagatsuma is a Member of the Institute of Electronics, Information and Communication Engineers (IEICE), Japan, the Technical Committee on Microwave Photonics of the IEEE Microwave Theory and Techniques Society, and the Microwave Photonics Steering Committee. He was the Recipient of the 1989 Young Engineers Award presented by the IEICE, the 1992 IEEE Andrew R. Chi Best Paper Award, the 1997 Okochi Memorial Award, the 1998 Japan Microwave Prize, the 2000 Minister's Award of the Science and Technology Agency, the 2004 Yokosuka Research Park Award, the 2006 Asia–Pacific Microwave-Photonics Conference Award, the 2006 European Microwave Conference Prize, the 2007 Achievement Award presented by the IEICE, the 2008 Maejima Award presented by the Post and Telecom Association of Japan, the 2009 Education and Research Award from Osaka University, the 2011 Commendation for Science and Technology by the Minister of Education, Culture, Sports, Science and Technology, the 2011 Recognition from Kinki Bureau of Telecommunications, Ministry of Internal Affairs and Communications, and the Asia–Pacific Microwave Conference Prize in 2002 and 2011.

Wojciech Knap obtained his M.S. and Ph.D. degrees from Faculty of Physics – Warsaw University Poland. His Ph.D. concerned the Terahertz (Far infrared) properties of narrow gap semiconductors HgTe and InSb. After his M.S. degree he obtained a Permanent Assistant Professor position at University of Warsaw Solid State Physics Department. In 1987 he left to France and worked at University of Montpellier, Grenoble High Magnetic Field Laboratory, Toulouse Pulsed High Magnetic Field Laboratory. In 1992 he obtained a permanent position at French National Center for Scientific Research - CNRS – Montpellier. Between 1999 and 2001 he worked (sabbatical) at USA – Rensellear Polytechnic Institute – at group of Prof. M. Shur. He obtained also a long term grant from Japan Society of Promotion of Science and spent a year in Prof. T. Otsuji group - Tohoku University 2007–2008. His main scientific interests and activities are: i) Fair Infrared-FIR (Terahertz - THz) properties of semiconductors: Investigation of absorption, detection and emission of Far Infrared (THz) radiation by free and shallow impurity bound carriers, ii) Quantum phenomena in transport: Weak localisation and anti-localisation and ballistic behaviour in low dimensional systems, and iii) Terahertz Plasma excitations in nanotransistors.